Physics Letters A 377 (2013) 582–586

Contents lists available at SciVerse ScienceDirect

Physics Letters A

www.elsevier.com/locate/pla

Optical gain spectra of unstrained graded GaAs/$Al_xGa_{1-x}As$ quantum well laser

E.L. Albuquerque [a], U.L. Fulco [a,*], M.S. Vasconcelos [b], P.W. Mauriz [c]

[a] Departamento de Biofísica e Farmacologia, Universidade Federal do Rio Grande do Norte, 59072-970 Natal, RN, Brazil
[b] Escola de Ciências e Tecnologia, Universidade Federal do Rio Grande do Norte, 59072-970 Natal, RN, Brazil
[c] Departamento de Física, Instituto Federal de Educação, Ciência e Tecnologia do Maranhão, 65020-300 São Luís, MA, Brazil

ARTICLE INFO

Article history:
Received 10 August 2012
Received in revised form 11 December 2012
Accepted 13 December 2012
Available online 28 December 2012
Communicated by R. Wu

Keywords:
Lasers
Quantum wells
Optical gain
Luttinger–Kohn method
Abrupt/non-abrupt interfaces

ABSTRACT

We have calculated the optical gain spectra in unstrained graded GaAs/$Al_xGa_{1-x}As$ single quantum well lasers as a function of the energy of the radiation, the quantum well width and the interface thickness. The optical gain spectra were calculated using the density matrix approach (Luttinger–Kohn method), considering the parabolic band model (conduction band), all subband mixing between the heavy and light holes (valence band), and the transversal electrical light polarization. Our results show that the optical peak gain is sensitive to the width and the graded profile of the interfaces, and is blue-shifted as a function of the interface width.

It is widely acknowledge that the importance of lasers is typically reflected due to their practical use in a large range of applications, as well as their highly controllable nonlinear coherent optical response [1,2]. To accomplish this task, there is a systematic effort nowadays, to reduce the required injection for the onset of lasing. This is done mainly by means of a dynamic exchange of energy between the carriers (electrons and holes) and photons in a resonant cavity, leading to relaxation oscillations, whenever the carrier population is perturbed by an external source such as an electrical injection or optical excitation [3,4].

In a semiconductor laser, relaxation oscillations give rise to deleterious effects, such as linewidth enhancement and chirp, due to the periodic modification of the refractive index in the active gain region by the carrier concentration modulation. Fortunately, these effects can be minimized by fabricating structures of reduced dimensionality, such as quantum wells, wires, and dots [5,6]. Other possibility is to take into account physical mechanisms that enhance stimulated emission, such as polaritons, allowing the development of a new generation of ultralow power and ultracompact room-temperature photonic devices [7–10]. The introduction of spin-polarized carriers may also present a valuable model system to elucidate the recombination of the carrier population, which plays an important role in the operation of a conventional laser [11]. Radiative recombination of spin-up and spin-down carriers in the active region of any semiconductor light source produces left- and right-circularly polarized light, respectively, giving rise to two equal and in-phase circularly polarized modes. Injection of spin-polarized carriers leads to emission of circularly or elliptically polarized light via the selection rules for radiative recombination [12,13].

Semiconductor lasers have been attractive for research because they are both physically very interesting and technologically important [14–16]. This is especially true for quantum well lasers, where it is possible to control the range, depth, and arrangement of the quantum mechanical potential wells, opening up the possibility to make very good devices [17–19]. The importance of the quantum well laser has steadily grown until today, where it is preferred for most semiconductor laser applications. This growing popularity is because, in almost every aspect, the quantum well laser is somewhat better than the conventional one with bulk active layers [20–22].

With the ability to grow different semiconductor layers epitaxially with atomic precision in thickness, the material bandgap can be designed to confine electrons in much the same way as described in standard quantum mechanics textbooks. This quantum confinement of the electron along the growth direction, significantly alters the band structure of the semiconductor, changing almost every property of the material to one degree or other [23]. The optical gain becomes dependent on the confinement characteristics of the semiconductor systems, in which the interfaces play a significant role.

* Corresponding author. Tel.: +55 84 32153793; fax: +55 84 32153791.
E-mail address: umbertofulco@gmail.com (U.L. Fulco).

0375-9601/$ – see front matter
http://dx.doi.org/10.1016/j.physleta.2012.12.025

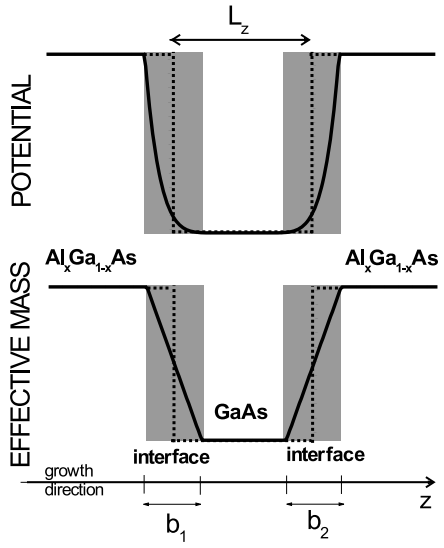

Fig. 1. Schematic illustration of the effective mass and potential energy of a GSQW (solid line) and of the equivalent abrupt ASQW (dotted line).

Investigations on the abrupt quantum well (QW) structures have been widely reported, although the use of less-abrupt interfaces in QW structures are relatively new. Recent works had shown the importance of using QWs with graded and less-abrupt interfaces in InGaN-based material systems, looking for improved spontaneous emission rate [24–26] and improved optical gain [27]. Besides, the improvement in quantum confined Stark effect had also been reported in Gaussian shape QWs [28], as well as the use of quantum well intermixing to form the less-abrupt interfaces leading to large blue-shift in emission wavelength [29].

The unstrained GaAs QWs structures are employed primarily as active regions for 850-nm diode lasers and vertical cavity surface emitting lasers, which are used as optical transmitters in datacom applications. However, several works considering compressively-strained InGaAsP QWs [30] and narrow InGaAs QWs [31] had been also used as improved active regions for achieving high performance 850-nm emitting lasers operating at high temperature with large differential gains attributed to their large compressive strain in the QWs. As a consequence, they depict very low-threshold current density [32] due to its large optical gain [33].

It is the aim of this work to describe a theoretical calculation of the optical gain in unstrained graded single quantum well (GSQW) lasers GaAs/$Al_xGa_{1-x}As$, as a function of the energy of the radiation, of the interface thickness, and of the width of the quantum well. We consider only the transversal electrical (TE) light polarization since, although straightforward, no new results are found for the simplest transversal magnetic (TM) light polarization. The theoretical calculation was done considering all subbands transitions in the quantum well. The results are compared with the equivalent abrupt single quantum well (ASQW) laser (see Fig. 1 for details of the geometries).

To calculate the energy levels of the electrons and holes confined into a GSQW/ASQW, we use the multi-band effective mass theory and the envelope-function approach together with a transfer-matrix technique. For simplicity, the conduction and valence bands are considered decoupled, as usual for most III–V semiconductors. We consider also the envelope functions to be slowly varying over the unit cells of the lattice, and the z-axis as the material growth direction. The effective mass and gap energy have a dependence on z in the quantum well interfaces whose profile, as depicted schematically in Fig. 1 for a GSQW (solid line), is [34]:

$$m_i(z) = m_0\big[\mu_{1i} + \mu_{2i}|z|\big], \tag{1}$$

$$V_i(z) = Q_i\big[1 + \varepsilon_1|z| + \varepsilon_2 z^2\big], \tag{2}$$

where m_0 is the free-electron mass, with $i = e$ (electrons), lh (light holes) and hh (heavy holes). Also, $\mu_{1e} = 0.067$, $\mu_{2e} = 0.083$; $\mu_{1lh} = 0.087$, $\mu_{2lh} = 0.063$; $\mu_{1hh} = 0.62$, $\mu_{2hh} = 0.14$, $\varepsilon_1 = 1.155$, and $\varepsilon_2 = 0.37$ are experimental parameters related with the dependence on the aluminium molar fraction x of the $Al_xGa_{1-x}As$ effective mass and energy gap, respectively, at the Γ-symmetry point [34]. Q_i is the band offset for the ith type of carrier, whose values taken from experiments are $Q_e = 0.6$, $Q_{hh} = Q_{lh} = 0.4$. Fig. 1 also shows the profile (dotted line) of the equivalent abrupt single quantum well (ASQW) used in this work.

Within the effective mass approximation and with the assumption that the conduction band is parabolic, the electron envelope function can be considered independent of $\vec{k}_t = (k_x, k_y, 0)$, the in-plane wave vector, which is perpendicular to the z-axis. The energy of an electron on the nth conduction subband can be written as:

$$E_{en}(k_t) = E_c + E_{en}(0) + \frac{\hbar^2 k_t^2}{2m_{av,e}}, \tag{3}$$

where E_c is the conduction band-edge energy, k_t is the magnitude of $\vec{k}_t = (k_x, k_y, 0)$ and $m_{av,e}$ is a weighted average of the bulk electron effective mass, defined as:

$$[m_{av,e}]^{-1} = \frac{\int_{-\infty}^{\infty} |F_{en}(z)|^2 [m_e(z)]^{-1}\, dz}{\int_{-\infty}^{\infty} |F_{en}(z)|^2\, dz}. \tag{4}$$

Here, $F_{en}(z)$ is the zone-center ($k_t = 0$) envelope function that describes the motion of the electron on the growth direction of the nth conduction subband. Also, $E_{en}(0)$ is the subband-edge energy ($k_t = 0$), which satisfies the one-dimensional Schrödinger-like equation

$$H_e(z) F_{en}(z) = E_{en}(0) F_{en}(z), \tag{5}$$

whose confinement Hamiltonian is given by

$$H_e(z) = -\frac{\hbar^2}{2}\frac{d}{dz}\left[\frac{1}{m_e(z)}\frac{d}{dz}\right] + V_e(z). \tag{6}$$

In the above equation, $m_e(z)$ and $V_e(z)$ are the effective mass and the confinement potential of the electron, respectively, which are dependent on the coordinate z at the interface, according to Eqs. (1) and (2). Eq. (5) can be solved numerically using a transfer-matrix technique [35].

For the calculation of the energy levels and envelope functions of the holes, we shall take into account the mixing of the subbands of the light hole and heavy hole in the valence band structure. This effect is well described by a multi-band effective mass approximation based on the $\vec{k}\cdot\vec{p}$ method of Luttinger and Kohn [36]. We adopt an analog effective Hamiltonian approach described in [37] to calculate the valence subband structure. In this approach, the hole envelope functions $F_{hn}(k_t, z)$, corresponding to the energy $E_{hn}(k_t)$ at any finite k_t, is expressed as a linear combination of the envelope functions at $k_t = 0$ in the following way:

$$F_{hn}(k_t, z) = \sum_{n'=1}^{4M} A_{n'n}(k_t) F_{hn'}(0, z). \tag{7}$$

Here, $h = hh, lh$, with the first index denoting a doubly degenerate group of heavy-hole subbands, and the second one denoting a doubly degenerate group of light-hole subbands. Also, M is the number of levels of the heavy/light holes, and $F_{hn}(0, z)$ is the zone-center ($k_t = 0$) envelope function, which describe the motion of the respective h-hole on the growth direction of the nth

valence subband. They are obtained by solving a one-dimensional Schrödinger-like equation, similar for the electron case (Eq. (5)).

In Eq. (7), n at the left-hand side represents the nth valence subband of the h-hole, while at the right-hand side is the nth eigenvector of the eigenvalue equation

$$H_{eff}A_n = E_nA_n, \tag{8}$$

where H_{eff} is the following effective Hamiltonian [38]:

$$H_{eff} = \begin{bmatrix} \tilde{E}_{hh} & \tilde{C}^T & \tilde{B}^T & 0 \\ \tilde{C}^* & \tilde{E}_{lh} & 0 & \tilde{B}^T \\ \tilde{B}^* & 0 & \tilde{E}_{lh} & \tilde{C}^T \\ 0 & \tilde{B}^* & \tilde{C}^* & \tilde{E}_{hh} \end{bmatrix}. \tag{9}$$

Here, the superscript T (*) means the transpose (adjoint) matrix. Also, $\tilde{E}_h$, $\tilde{B}$ and $\tilde{C}$ are $M \times M$ submatrices, whose matrix elements are given by:

$$C_{nn'} = \frac{\hbar^2\sqrt{3}}{2m_0}\gamma(x)k_t^2e^{-2i\phi}\int_{-\infty}^{+\infty} dz\, F^*_{hh,n}(0,z)F_{lh,n'}(0,z), \tag{10}$$

$$B_{nn'} = -\frac{\hbar^2\sqrt{3}}{m_0}\gamma(x)k_te^{i\phi}\int_{-\infty}^{+\infty} dz\, F^*_{hh,n}(0,z)\frac{\partial}{\partial z}F_{lh,n'}(0,z), \tag{11}$$

$$E_{hh,nn'} = \delta_{nn'}E_{hh,n}(0) - \frac{\hbar^2k_t^2}{2m^t_{av,hh}}, \tag{12}$$

$$E_{lh,nn'} = \delta_{nn'}E_{lh,n}(0) - \frac{\hbar^2k_t^2}{2m^t_{av,lh}}. \tag{13}$$

In the above equations, $n, n' = 1, 2, \ldots, M$, $E_{h,n}(0)$ denote the nth subband-edge ($k_t = 0$) energy of the h-hole (the origin of the energy is taken at the top of the conduction band), and $\gamma(x)$ is the Luttinger parameter in the $Al_xGa_{1-x}As$ [39], defined by

$$14\gamma(x) = x\gamma(\text{AlAs}) + (1-x)\gamma(\text{GaAs}), \tag{14}$$

with $\gamma(\text{AlAs}) = 0.82$ and $\gamma(\text{GaAs}) = 2.06$ [40]. Besides, ϕ is a phase angle, defined as $\phi = \tan^{-1}(k_y/k_x)$, and $m^t_{av,h}$ is a weighted average of the h-hole effective mass in the transversal direction, defined in a similar way as in Eq. (4).

The H_{eff} Hamiltonian defined in Eq. (9) is considered to be an axial approximation of the Luttinger–Kohn Hamiltonian, which implies that the subband energy dispersion relations are independent of the angle ϕ.

In order to calculate the optical gain, we need to determine first the quasi-Fermi levels at the conduction band and valence band E_{fc} and E_{fv}, respectively. We found it by imposing the charge neutrality in the material for a given carriers density. The carrier densities on the conduction and valence bands, N and P, respectively, for a given quasi-Fermi levels, are obtained by integrating the density of states multiplied by the occupation probability over the quasi-entire bands, as follows:

$$N = \sum_n 2\int_{E_{en}(0)}^{E_{fc}} \rho^{2D}_{en}(E)f_c(E)\,dE, \tag{15}$$

and

$$P = \sum_h\sum_{n'} 2\int_{E_{fv}}^{E_{hn'}(0)} \rho^{2D}_{hn'}(E)\big[1 - f_v(E)\big]\,dE, \tag{16}$$

where

$$f_{c(v)}(E) = \frac{1}{1 + \exp[(E - E_{fc(fv)})/k_BT]}. \tag{17}$$

The sum over h is required to consider the contributions from the heavy- and light-hole subbands. The $\rho^{2D}(E)$ is the two-dimension density of states function, which is assumed to be [17]

$$\rho^{2D}_{en(hn')}(E) = \frac{m_{e(h)}H[E - E_{en(hn')}(0)]}{2\pi\hbar^2L_z}, \tag{18}$$

where $H[E - E_{en(hn')}(0)]$ is the Heaviside step function.

The optical gain spectra at a particular photon energy and in-plane wave vector magnitude, for a symmetrical potential, can be given by [41]:

$$g(E) = \left(\frac{e^2\hbar}{\eta_r c\epsilon_0 m_0^2 L_z}\right)\left(\frac{1}{E}\right)\sum_{h,n,n'}\int k_t\,dk_t\big|M^T_{nn'}(k_t)\big|^2 \times \delta\big(E - E^{en}_{hn'}(k_t)\big)\big[f_{en}(k_t) - f_{hn'}(k_t)\big], \tag{19}$$

where E is the photon energy, η_r is the refractive index in the GaAs, e is the electron charge, ϵ_0 is the free-space permittivity, c is the speed of light, m_0 is the free-electron mass, L_z is the equivalent abrupt single quantum well width, and $|M^T_{nn'}(k_t)|^2$ is the transition matrix element. Also, $f_{en}(k_t)$ and $f_{hn'}(k_t)$ are the Fermi occupation probabilities of the n- and n'-levels in the conduction and valence bands, respectively, and are defined by

$$f_{en(hn')}(k_t) = \frac{1}{1 + \exp[(E_{en(hn')}(k_t) - E_{fc(fv)})/k_BT]}. \tag{20}$$

In Eq. (19), $E^{en}_{hn'}(k_t) = E_g + E_{en}(k_t) - E_{hn'}(k_t)$; E_g is the GaAs gap energy and $E_{en}(E_{hn'})$ is the transition energy. The transition matrix element, which gives the relative strength of the various optical transitions, under axial approximation is given by [17]:

$$\big|M^{TE}_{nn'}(k_t)\big|^2 = \left[\big|\langle F_{en}|F_{hh,n'}(k_t)\rangle\big|^2 + \frac{1}{3}\big|\langle F_{en}|F_{lh,n'}(k_t)\rangle\big|^2\right]|M_b|^2, \tag{21}$$

for TE polarization (the optical electric field is polarized in the xy-plane). The magnitude of the bulk matrix element $|M_b|^2$ is known experimentally. For GaAs material, $6|M_b|^2/m_0 = 25.0$ eV [18].

To include the spectral broadening in each transition caused by all sources of the electron scattering, we convolve the expression for the optical gain with some spectral line shape function over all transition energies E. Choosing a Lorentzian line shape function for the optical gain analysis [42], it can be written as:

$$G(E) = \int g(E')L(E' - E)\,dE', \tag{22}$$

where

$$L(E' - E) = \frac{\Gamma/(2\pi)}{(E' - E)^2 + (\Gamma/2)^2} \tag{23}$$

is the Lorentzian. In this expression, Γ is the width at the half maximum gain spectra, and is about 6 meV [38]. It is related at the intraband relaxation time, τ_{in} (~ 0.1 ps), as $\Gamma/2 = \hbar/\tau_{in}$ [43].

Fig. 2 shows a 3D plot of the optical gain spectra considering a 8 nm unstrained non-abrupt $GaAs/Al_{0.2}Ga_{0.8}As$ graded single QW (GSQW) laser as a function of the photon energy and of the interface width. The non-abrupt GaAs/AlGaAs QWs is justified since the existence of micro-roughness superimposed to macro-roughness gives rise to the existence of graded interfaces in semiconductor heterostructures. Even in systems such as GaAs/AlGaAs QWs, the thickness of the graded interface regions is at least of the order of three monolayers [38], which is enough to have an effect on the laser optical gain, as it is illustrated in Fig. 2. Besides, although the

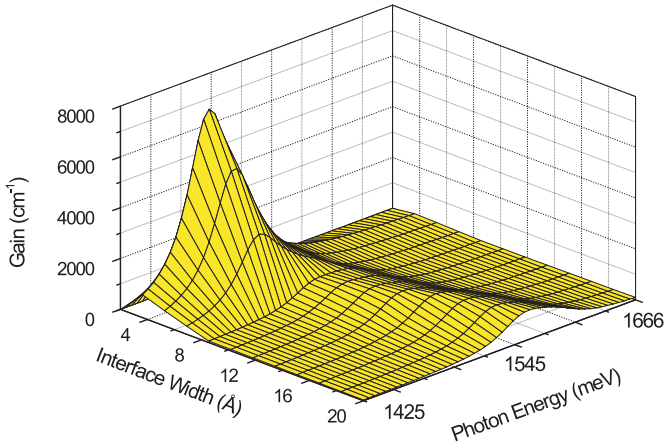

Fig. 2. (Color online.) A 3D optical gain spectra of a 8 nm GaAs/$Al_{0.2}Ga_{0.8}As$ QW laser as a function of the photon energy and of the interface width. Observe the appearance of a large blue-shift as the interface width increases.

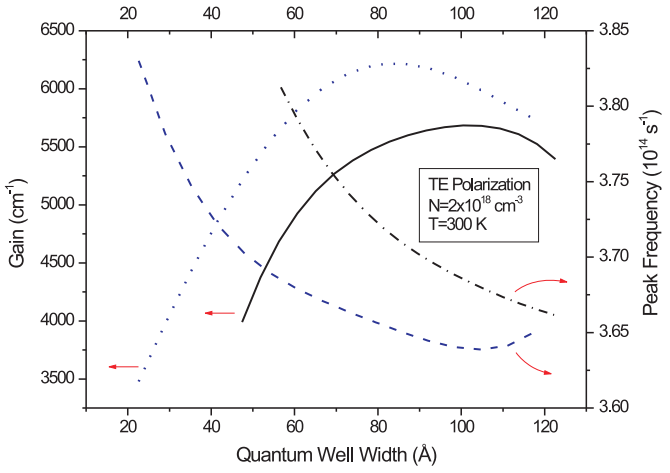

Fig. 3. (Color online.) The gain peak of a GSQW laser (solid line) GaAs/$Al_{0.2}Ga_{0.8}As$, with 4 Å of interface width, and its equivalent ASQW laser (dotted line). Also shown are their corresponding peak frequencies (dashed line and dashed–dotted line, respectively) as a function of the quantum well width (see the right-hand side scale).

electron's low energies in a quantum well may be sensitive to the strain effects, it can be ignored for higher-frequency [44], as those considered in this work.

The optical gain was calculated for a TE electric light polarization with relaxation at room-temperature (300 K), and an adopted carrier density $N = 2 \times 10^{18}$ cm^{-3}. Furthermore, a linear (parabolic) dependence with coordinate z of the effective mass (potential profile) on the interface was taken into account. As a result, the increase of the interface width leads to large and unexpected blue-shift of the gain's peak, representing an important step in the characterization of a new generation room-temperature photonic devices.

Fig. 3 depicts the optical gain's peak of a non-abrupt GaAs/$Al_{0.2}Ga_{0.8}As$ QW laser, with 4 Å of interface width, and its corresponding frequency, as a function of the quantum well width for a carrier density $N = 2 \times 10^{18}$ cm^{-3} at room temperature ($T = 300$ K) and TE electric light polarization. For completeness, it is also shown the gain's peak and peak frequency for an abrupt equivalent single QW (ASQW) laser. Observe a blue-shift of the gain's peak in the interval that goes from 45 to 100 Å (20 to 80 Å) and a red-shift of the peak frequency, for the GSQW (ASQW) laser. Observe also a maximum of the gain's peak at 100 Å and 80 Å for the GSQW and its equivalent ASQW lasers.

In conclusion, we have formulated a theoretical analysis to study the effect of non-abrupt interface on the optical gain of a quantum well laser. The key observation was a large blue-shift of the gain's peak at room-temperature as the interface width increases. As a consequence, for an improved description of the optical gain in quantum confined based semiconductor lasers, it is necessary to take into account interface effects, as the results of the present work indicate. On the experimental side, interface characterization of actual laser samples, together with measurements on the frequency dependence of their optical gain, hopefully will allow the confirmation for the role of the interfaces on the optical laser gain, as predicted by our calculations.

Acknowledgements

This work was partially financed by the Brazilian Research Agencies CAPES (PROCAD, Rede NanoBioTec and PNPD), CNPq (NCT-Nano(Bio)Simes, Project No. 573925/2008-9, and Casadinho/Procad) and FAPERN/CNPq (Pronex).

References

[1] S.L. Chuang, Physics of Optoelectronic Devices, 2nd ed., Wiley, New York, 2009.
[2] M.A. Parker, Physics of Optoelectronics, CRC Press, New York, 2004.
[3] K.Y. Lau, N. Bar-Chaim, I. Ury, Ch. Harder, A. Yariv, Appl. Phys. Lett. 43 (1983) 1.
[4] H. Dery, G. Eisenstein, IEEE J. Quantum Electron. 40 (2004) 1398.
[5] J. Lee, R. Oszwaldowski, C. Gothgen, I. Zutic, Phys. Rev. B 85 (2012) 045314.
[6] M. Holub, J. Shin, D. Saha, P. Bhattacharya, Phys. Rev. Lett. 98 (2007) 146603.
[7] A. Das, J. Heo, M. Jankowski, W. Guo, L. Zhang, H. Deng, P. Bhattacharya, Phys. Rev. Lett. 107 (2011) 066405.
[8] D. Bajoni, P. Senellart, E. Wertz, I. Sagnes, A. Miard, A. Lemaître, J. Bloch, Phys. Rev. Lett. 100 (2008) 047401.
[9] M.S. Vasconcelos, P.W. Mauriz, F.F. de Medeiros, E.L. Albuquerque, Phys. Rev. B 76 (2007) 165117.
[10] H. Deng, G. Weihs, D. Snoke, J. Bloch, Y. Yamamoto, Proc. Natl. Acad. Sci. USA 100 (2003) 15318.
[11] D. Saha, D. Basu, P. Bhattacharya, Phys. Rev. B 82 (2010) 205309.
[12] J. Rudolph, S. Dohrmann, D. Hagele, M. Oestreich, W. Stolz, Appl. Phys. Lett. 87 (2005) 241117.
[13] C.H. Li, G. Kioseoglou, O.M.J. van't Erve, M.E. Ware, D. Gammon, R.M. Stroud, B.T. Jonker, R. Mallory, M. Yasar, A. Petrou, Appl. Phys. Lett. 86 (2005) 132503.
[14] Z.I. Alferov, Rev. Mod. Phys. 73 (2001) 767.
[15] V.M. Ustinov, A.E. Zhukov, A.Yu. Egorov, N.A. Maleev, Quantum Dot Lasers, Oxford University Press, New York, 2003.
[16] D. Bimberg, M. Grundmann, N.N. Ledentsov, Quantum Dot Heterostructures, Wiley, New York, 1999.
[17] P.S. Zory Jr., in: Quantum Well Lasers, Academic Press, 1993.
[18] S.L. Chuang, in: Physics of Optoelectronic Devices, Wiley–Interscience, 1995.
[19] P. Bhattacharya, Semiconductor Optoelectronic Devices, Prentice Hall, Englewood Cliffs, NJ, 1996.
[20] G. Tandoi, C.N. Ironside, J.H. Marsh, A.C. Bryce, IEEE J. Quantum Electron. 48 (2012) 318.
[21] S.D. Wu, L. Wan, J. Appl. Phys. 110 (2011) 123109.
[22] N. Hossain, S.J. Sweeney, S. Rogowsky, R. Ostendorf, J. Wagner, S. Liebich, M. Zimprich, K. Volz, B. Kunert, W. Stolz, Electronics Lett. 47 (2011) 931.
[23] S.R. Chinn, P.S. Zory, A.R. Reisinger, IEEE J. Quantum Electron. 24 (1988) 2191.
[24] H. Zhao, G. Liu, X.-H. Li, G.S. Huang, J.D. Poplawsky, S.T. Penn, V. Dierolf, N. Tansu, Appl. Phys. Lett. 95 (2009) 061104.
[25] H.P. Zhao, G.Y. Liu, X.H. Li, R.A. Arif, G.S. Huang, J.D. Poplawsky, S. Tafon Penn, V. Dierolf, N. Tansu, IET Optoelectronics 3 (2009) 283.
[26] H. Zhao, G. Liu, J. Zhang, J.D. Poplawsky, V. Dierolf, N. Tansu, Optics Express 19 (2011) A991.
[27] H. Zhao, N. Tansu, J. Appl. Phys. 107 (2010) 113110.
[28] A. Ramirez-Morales, J.C. Martínez-Orozco, I. Rodríguez-Vargas, J. Appl. Phys. 110 (2011) 103715.
[29] B.S. Ooi, K. McIlvaney, M.W. Street, A.S. Helmy, S.G. Ayling, A.C. Bryce, J.H. Marsh, J.S. Roberts, IEEE J. Quantum Electron. 33 (1997) 1784.
[30] N. Tansu, D. Zhou, L.J. Mawst, IEEE Photon. Technol. Lett. 12 (2000) 603.
[31] E.P. O'Reilly, J.S. Gustavsson, P. Westbergh, A. Haglund, A. Larsson, A. Joel, IEEE J. Quantum Electron. 46 (2010) 506.
[32] N. Tansu, J.Y. Yeh, L.J. Mawst, Appl. Phys. Lett. 82 (2003) 4038.
[33] G. Tsvid, J. Kirch, L.J. Mawst, M. Kanskar, J. Cai, R.A. Arif, N. Tansu, P.M. Smowton, P. Blood, IEEE J. Quantum Electron. 44 (2008) 732.
[34] S. Adachi, J. Appl. Phys. 58 (1985) R1.
[35] Y. Ando, T. Itoh, J. Appl. Phys. 61 (1987) 1497.

[36] J.M. Luttinger, W. Kohn, Phys. Rev. 97 (1955) 869.
[37] K.S. Chan, J. Phys. C: Solid State Phys. 19 (1986) L125.
[38] K.S. Chan, E.H. Li, M.C.Y. Chan, IEEE J. Quantum Electron. QE-34 (1998) 157.
[39] E.H. Li, B.L. Weiss, K.S. Chan, Phys. Rev. B 46 (1992) 15181.
[40] I. Vurgaftman, J.R. Meyer, L.R. Ram-Mohan, J. Appl. Phys. 89 (1992) 5815.
[41] O. Gilard, F. Lozes-Dupuy, G. Vassilieff, S. Bonnefont, P. Arguel, J. Barrau, P. Le Jeune, J. Appl. Phys. 86 (1999) 6425.
[42] M. Asada, IEEE J. Quantum Electron. QE-25 (1989) 2019.
[43] M. Yamada, Y. Suematsu, J. Appl. Phys. 52 (1981) 2653.
[44] Jun-jie Shi, Phys. Rev. B 68 (2003) 165335.